Design and compressive behavior of controllable irregular porous scaffolds: based on Veronoi-tessellation and for additive manufacturing

Article (Accepted Version)

Design and Compressive Behavior of Controllable Irregular Porous Scaffolds: Based on Voronoi-Tessellation and for Additive Manufacturing

Guanjun Wang,[1,2] Lida Shen,[1] Jianfeng Zhao,[*,1] Huixin Liang,[1] Deqiao Xie,[1] Zongjun Tian[1] and Changjiang Wang[3]

[1]*College of Mechanical and Electrical Engineering, Nanjing University of Aeronautics and Astronautics, 29 Yudao Street, Nanjing 210016, PR China*

[2]*Suzhou Kangli Orthopedics Instrument Co. Ltd., Luyuan Tangqiao Town, Zhangjiagang Suzgou, 215600 PR China*

[3] *Department of Engineering and Design, University of Sussex, Sussex House, Brighton BN1 9RH, United Kingdom*

*Corresponding Author E-mail: zhaojf@nuaa.edu.cn

Abstract

Adjustments of the mechanical properties (apparent elastic modulus and compressive strength) in porous scaffolds is important for artificial implants and bone tissue engineering. In this study, a top-down design method based on Voronoi-Tessellation was proposed. This method was successful in obtaining the porous structures with specified and functionally graded porosity. The porous specimens were prepared by selective laser melting technology. Quasi-static compressive tests were conducted as well. The experiment results revealed that the mechanical properties were affected by both porosity and irregularity. This is different from the traditional prediction model that only considers a single porosity. The results also indicated a threshold effect of

the strength enhancement at high levels of irregularity. The method proposed in this study provides an efficient approach for the bionic design and topological optimization of scaffolds.

1. Introduction

Long-term aseptic loosening of artificial implants and refracture are fatal complications within the clinical setting .[1,2] The main issue within artificial implants is 'stress shielding'. Stress is unable to adequately transfer from the metal implant device to the bone. This is caused by the large difference between their elastic moduli. Osteocytes that do not have adequate stress stimulation will die and be absorbed, which results in the loosening of implants and sometimes fracturing occurs. Porous structures were introduced to the implant devices to stop these occurrences. These structures could reduce the apparent elastic modulus to the level of human bones (4 Gpa $\sim$ 30 Gpa).[1,2] The porous structures also provide necessary space for osteocyte and transport pathways of tissue fluid. This is conductive to biological fixation between the bone and implant.[3–5] Metal implants with porous structures could be fabricated rapidly and precisely as additive manufacturing (AM) has become more developed. The selective laser melting (SLM) and the electron beam melting (EBM) are the most popular methods within AM. Designing porous scaffolds that could meet both structural and mechanical properties requirements has become necessary.[6]

The morphology of these porous structures are broadly divided into regular or irregular structures. The primary construction methods of the regular porous structures are the cell unit method [7] and the triply periodic minimal surface method.[8] The regular porous scaffolds have regular pore morphology, good connectivity, and controllable mechanical properties. This results in their wide application.[9] Irregular porous scaffolds are typically implemented by computer programs and mathematical models.[10–12] The irregular porous scaffolds enable geometric and mechanical parameters to be designed precisely or distributed in a gradient manner. Furthermore, Irregular porous scaffolds have the ability to simulate the complex

and anisotropic microstructures of bone tissues. This provides additional freedom within bionic design and topological optimization.[13–15] The design approach for irregular porous structure is another key technology that requires additional research.

Unfortunately, most of previous studies on irregular porous structures ignored the effect of irregularity and its evolution. Uncontrollable irregularity lead to poor repeatability of morphology and the mechanical properties. In this study, we proposed a top-down design method (probability sphere method) based on the Voronoi-Tessellation method to construct controllable porous scaffolds. The probability sphere method uses a regular three-dimensional point array that is agitated by probability spheres. This generates the irregular but controllable porous scaffold. In order to evaluate the porous scaffolds, we prepared two sets of specimens by SLM. We then measured their geometric parameters with industrial CT (Computer Tomography). Their mechanical parameters were tested with quasi-static compressive experiments.

2. Materials and Methods

2.1 Modeling and characterization of porous scaffolds

The Voronoi-Tessellation is a method of space partition, based on the seed point .[16] The Voronoi diagram is defined below:

For a set of points on the m-dimensional Euclidean space

$$P = \{p_1, \ldots, p_n\} \subset R^m, 2 \leq n < \infty, p_i \neq p_j, i, j \subset I_n = \{1, \ldots, n\} \tag{1}$$

The line between p_i and p_j divides the space into two parts, $H_i(p_i p_j)$ is the part including p_i, then,

$$V(p_i) = \{x | \|x - p_i\| \leq \|x - p_j\|\} = \bigcap_{j \in I_n \setminus \{i\}} H(p_i, p_j) \tag{2}$$

is the m-dimensional Voronoi generated by p_i on R^m space , $\gamma(p) = \{V(p_i), ..., V(p_n)\}$ is

called the Voronoi diagram and p_i is the seed point. Voronoi diagram is determined by the amount and the distribution of seed points. The control of the seed points is paramount to successful irregular porous scaffolds modeling. Previous researches have preferred to generate three dimensional points in random manner.[17–20] However, there is little control of these random points and the morphology and the mechanical properties have poor repeatability. The proposed method considers both 'irregularity' and 'controllability'. An ordered cube lattice was generated using CAD software Grasshopper® (Version 0.9.0076). There were n layers within the cube lattice. The distance between the two adjacent points within Layer i was b_i, as seen in Fig. 1. Denote the point on Line m and Column n in Layer i as P_{mn_i}. Denote the space between Layer $(i-1)$ and Layer i as a_i. The spherical regions were centered at each point and generated with the radius of R_i. A new point P'_{mn_i} was then generated randomly in each spherical region to replace their predecessors. This formed the new lattice. P'_{mn_i} was generated as follows:

$$\begin{cases} x' = x + R \times rand \times \sin(\pi \times rand) \times \cos(2\pi \times rand) \\ y' = y + R \times rand \times \sin(\pi \times rand) \times \cos(2\pi \times rand) \\ z' = z + R \times rand \times \sin(\pi \times rand) \times \cos(2\pi \times rand) \end{cases} \tag{3}$$

Where, *rand* is a random function with uniform distribution in [0, 1].

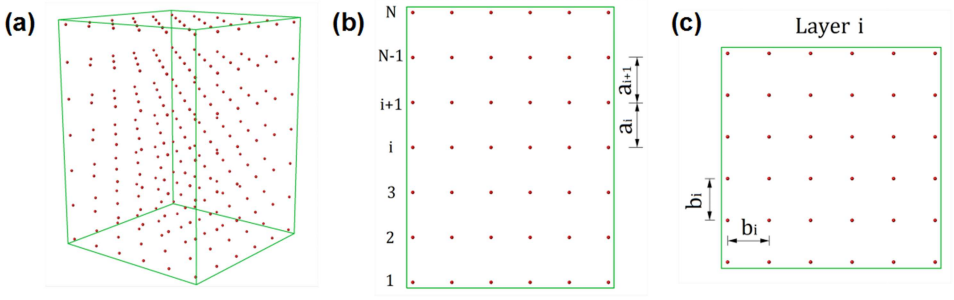

Figure 1: Regular lattice. (a) Perspective view. (b) Front view. (c) Top view of Layer i.

Irregularity coefficient was defined as ε:

$$\varepsilon = \frac{1}{N} \sum_{m,n,i} \frac{\left| \overrightarrow{P_{mn\_i} P'_{mn\_i}} \right|}{a_i} \tag{4}$$

Where, N is the number of points in the irregular lattice generated previously, $0 \leq \varepsilon < 1$.

The radius of spherical region R_i was constrained to increase the controllability of the irregular lattice by $0 < R_i \leq \frac{1}{2} a_i$. The Voronoi cells were generated in Grasshopper® following the irregular lattice generation. The struts were generated based on the edges of the Voronoi cells. Then, a Boolean operation was used to form a porous scaffold with a specific shape, as shown in Fig. 2. The size of the pores and struts were controlled by introducing the scale coefficient K. This was the ratio of a pore area to the corresponding surface area of the cell $K = \frac{S_{ci}}{S_{pi}}$, as shown in Fig. 3. K controls both diameters of the pores and the struts. When the seed points are given, the diameters of the pores and struts could be adjusted by K.

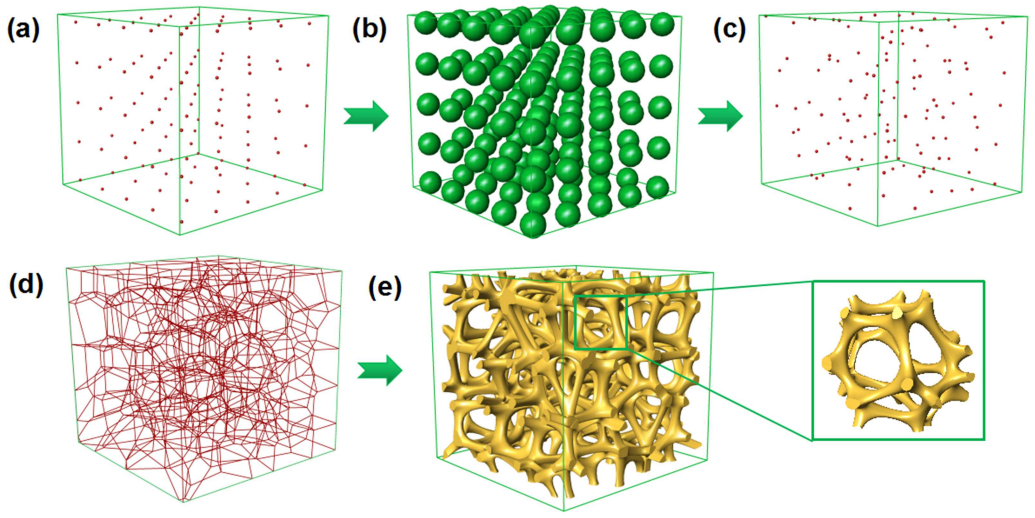

Figure 2: The design principle of porous scaffold. (a)Designing regular lattice. (b)Generating probability spheres.(c)Obtaining irregular lattice. (d)Generating voronoi cells based on irregular lattice.(e)Constructing porous structures.

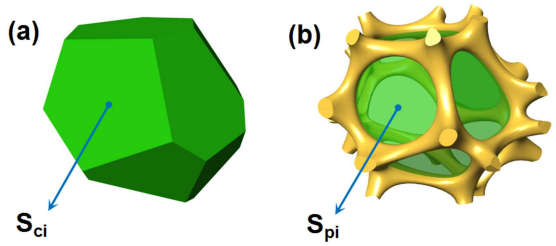

Figure 3: The definition of scale coefficient K. (a) One of the Voronoi cell. (b) Porous structure based on (a).

The gradient distribution of the points in the Z axis were obtained. This allowed one to obtain the gradient distribution of porosity in the direction of Z axis, as shown in Fig. 4. K was then replaced with linear variables that related to cell position:

$$K = \frac{Z_t - Z_b}{K_t - K_b} + K_b - \frac{Z_t - Z_b}{K_t - K_b} \times Z_b \tag{5}$$

Where, Z_b and Z_t denoted the minimum and the maximum of the Z axis coordinate of body center of all the voronoi cells. K_b and K_t represented the minimum and maximum of the value of K. In order to fit the gradient distribution of points, the radius of probability sphere was set as $R_i = \frac{1}{2}a_i$. Based on the probability sphere method, Fig. 5 shows the process of constructing the artificial bone with porous gradient structures.

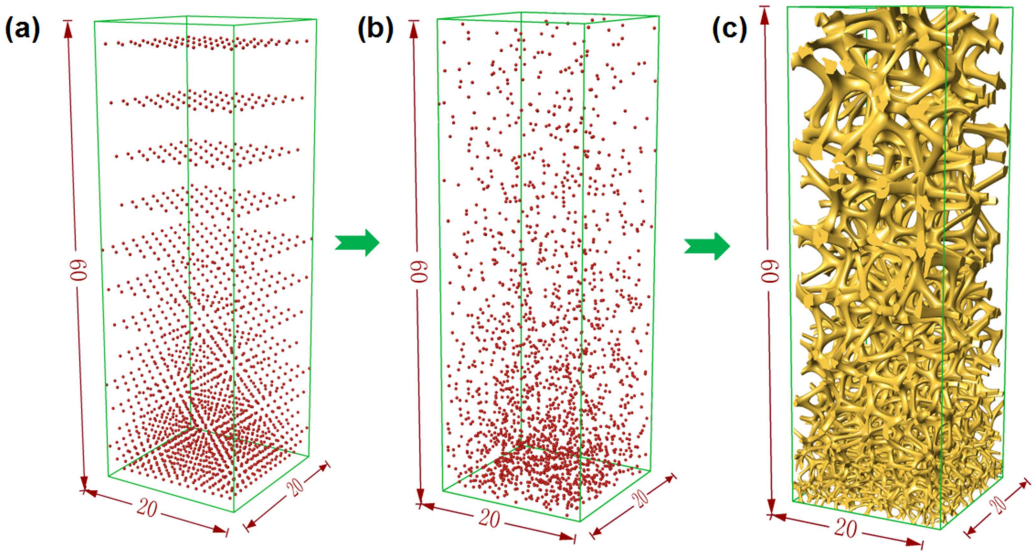

Figure 4: The modeling method of porous scaffold with gradient porosity. (a) The regular lattice. (b) The irregular lattices. (c) Porous scaffolds with gradient distribution of porosity ($K_t = 0.9$, $K_b = 0.7$).

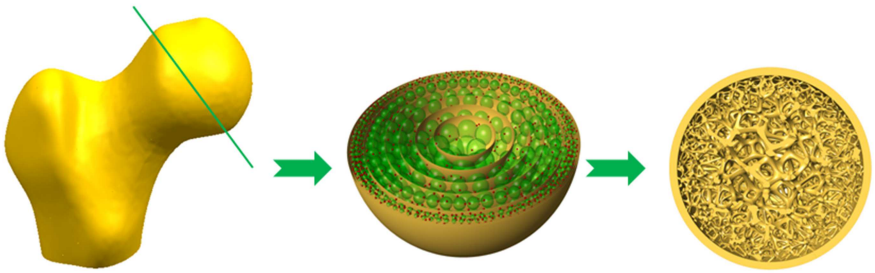

Figure 5: The method of constructing the artificial bone with porous gradient structures: Firstly, offset the surface by incremental distances; Secondly, generate spherical regions based on the intersection points of UV isocurves; Thirdly, generate irregular lattice then construct porous gradient structures.

The parameters of the porous scaffold included pore size, porosity, and strut diameter. The porosity in the geometric model was calculated by the formula $\Phi = \left(1 - \frac{V_P}{V}\right) \times 100\%$, where Φ is porosity, V_P is the volume of the porous scaffold, and V is outer volume of the porous scaffold.

The sections at the midpoint of the strut sections were extracted. The equivalent diameter method was used to calculate the pore diameters when the area was equivalent to the sections.

The equivalent diameter method was used to calculate the aperture, as shown in formula (6).

$$D = \frac{1}{n_D} \sum_{i=1}^{n} \frac{4S_i}{\pi}, d = \frac{1}{n_d} \sum_{i=1}^{n} \frac{4A_i}{\pi} \tag{6}$$

Where, n_D is the number of pores, n_d is the number of struts, D is the equivalent aperture, S_i is the hole area, d is the equivalent strut diameter, and A_i is the cross-sectional area of strut.

2.2. Fabrication and compressive testing

The porous specimens were fabricated with an SLM machine (M290, EOS GmbH, Germany) using the optimized processing parameters that were provided by the manufacturer. The materials were commercial Ti6Al4V ELI, supplied by EOS GmbH. The average particle size was approximately 30 μm.

The factors that influenced the mechanical properties of the porous scaffolds included porosity, pore diameter, strut diameter, and shape of the strut section. Porosity is thought to be the most influential factor .[21] Irregularity is another important parameter within irregular porous scaffolds. In this paper, two sets of experiments were conducted to investigate the effects of porosity and irregularity on the mechanical properties of porous scaffolds. The design parameters of the porous scaffold are shown in Table 1.

Table 1: Design parameters of porous scaffolds

Set	N	K	R
Porosity	125	0.65	1
		0.7	1
		0.75	1
		0.8	1
		0.85	1
		0.9	1
Irregularity	125	0.8	0.4
		0.8	0.8
		0.8	1.2
		0.8	1.4
		0.8	1.6
		0.8	1.8

Resolutions from 9.68 μm to 15.34 μm were performed by an industrial CT (XTH225, Nikon, Japan) to scan the porous scaffolds. A 3D model of the porous scaffolds was reconstructed to measure the porosity in software. The compression tests of specimens were conducted with a mechanical testing machine (CMT5105, MTS System Corporation, America). The crosshead displacement speed was fixed at 0.25 mm/min.

3. Results and discussion

3.1. Controllability of geometric parameters

Fig. 6 shows lattices and corresponding porous scaffolds with different regularities. Fig. 7 depicts the relationship between the irregularity (ε) and radius (R) of probability spheres. The porous scaffolds increase in irregularity as ε grows. There was a good linear relationship between R and ε. This suggests that the probability sphere method could control and characterize the degree of irregularity of porous scaffold.

In theory, the irregular coefficient ε defined in this paper does not fully characterize the true degree of irregularity of the points. For example, if all vectors $|\overrightarrow{p_i p_i}|$ were unidirectional, although the value of ε could be huge, the degree of irregularity of the lattice would not

change. There is little prospect of such special case occurring in practical experiments. As a result, the irregular coefficient ε meets the application requirements.

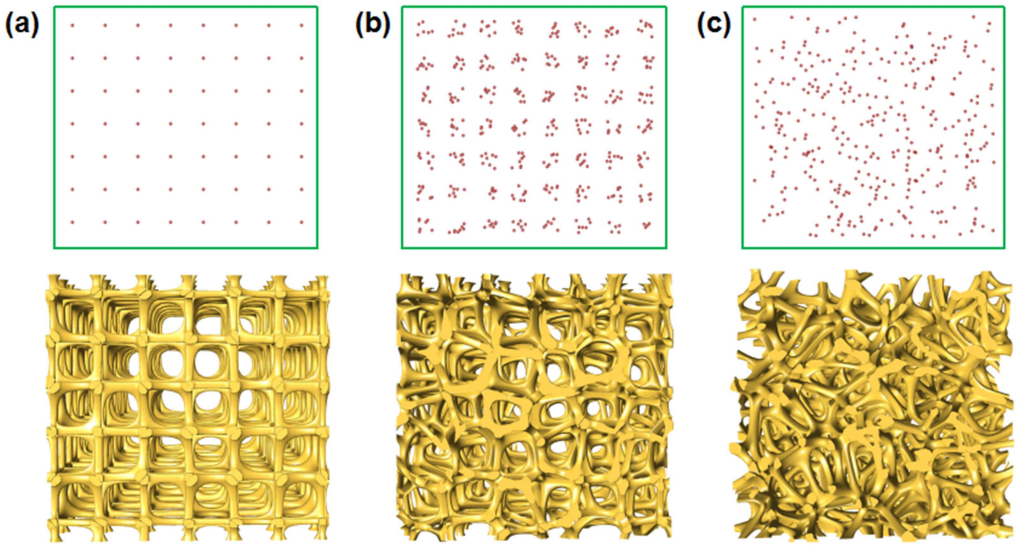

Figure 6: Porous structures with different irregularities. (a) $\varepsilon = 0.06$. (b) $\varepsilon = 0.25$. (c) $\varepsilon = 0.86$. ($K = 0.9$, $N = 512$).

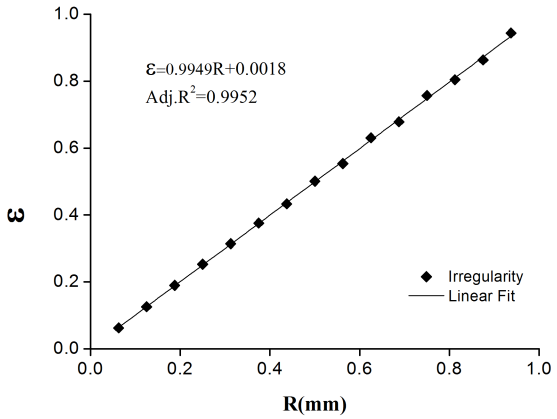

Figure 7: Relationship between R and ε.

Figs. 8 and 9 show the effect of the amount of the seed points (N) and scale coefficient (K) on geometric parameters. N had little effect on Φ. The overall fluctuation range was less than 10%. The larger N was, the less the effect of it had on Φ. A power relation existed between N and D or d. There were strongly linear relation between $K$and Φ, as well as D and d. K had more greater effect on geometric parameters than N. The primary factor that

ffected the geometric parameters of porous scaffolds was K.The standard for the proper size of bone cell ingrowth is 200 μm to 1200 μm.[6,22] The method presented in this paper adjusted N, K and R to be within this scope.

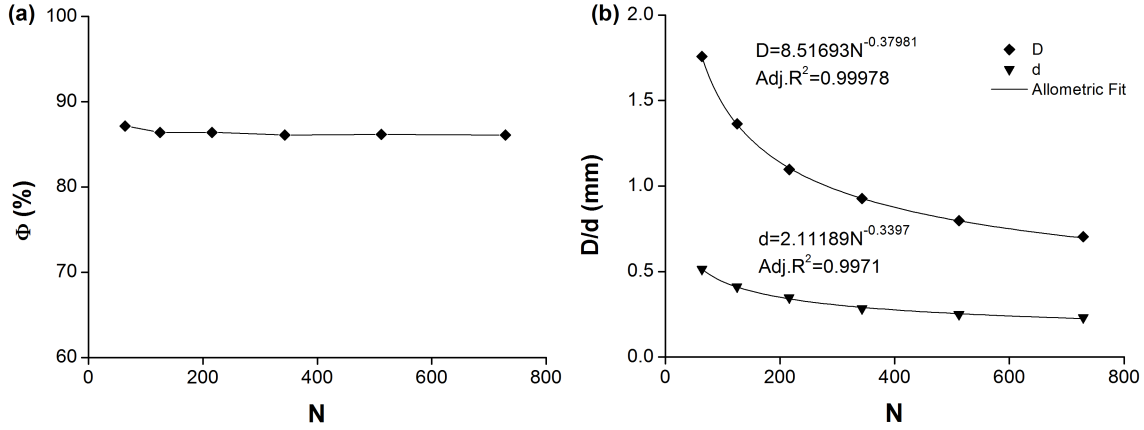

Figure 8: The relation between points and (a) porosities, and (b) diameters of pores and struts. ($K = 0.8$, $R = 0.5$).

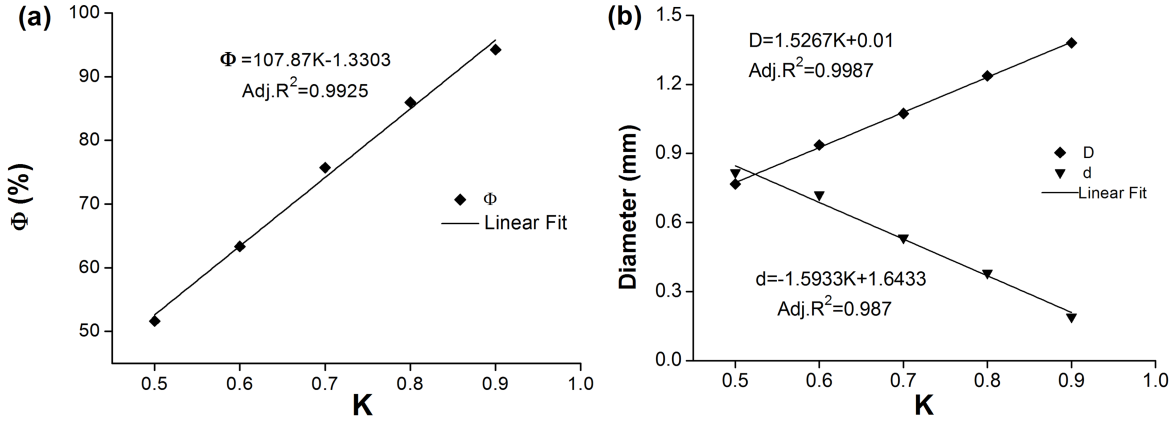

Figure 9: The relation between scale coefficients and (a) porosities, and (b) diameters of pores and struts. ($N = 216$, $R = 0.5$).

3.2. Controllability of gradient porosity

Table 2 shows the four groups of K_b and K_t (see fig 4). These groups were set to explore the influence of different combinations on the gradient change of porosity. The slope of the best fit line was defined as the porosity gradient G. Fig. 10 shows the gradient variation of the porosity as it related to height. As seen in Fig. 10, the porosity changed linearly, in the

height direction which corresponded with K. When K_t remained constant, the maximum porosity remained constant as well (the porosity at the top of the structure). This further confirmed that porosity was primarily determined by K in 3.1.

Table 2: Scale coefficients for gradient porosity

Groups	K_t	K_b	G
1	0.9	0.6	0.54
2	0.9	0.7	0.34
3	0.9	0.8	0.16
4	0.9	0.9	0.03

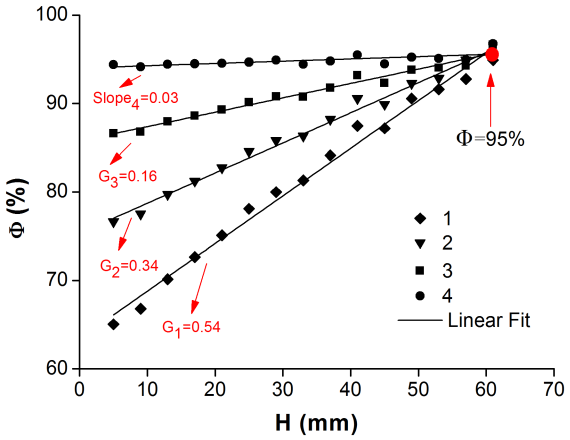

Figure 10: Porosity gradient corresponding to the different sets of scale coefficients.

3.3. Controllability of mechanical properties

Fig. 11 illustrates porous structures that were prepared by SLM technology. Table 3 lists the contrast between the design porosity and the as-built porosity. The porosity deviations between the models and the specimens were less than 4%. This met the requirements of high-precision manufacturing of porous scaffolds. Fig. 12 shows the the relationship between porosity Φ, apparent elastic E modulus, and compressive strength S. There was a power function relationship between the S and Φ, as well as a strong linear relationship between E and Φ (Fig. fig12). Fig. 13 shows the relation between irregularity, elastic modulus, and compressive strength. As ε, increased, E decreased linearly. The compressive strength

showed a downward trend at low levels of irregularity ($0 \sim 0.34$). The strengths of the structures were enhanced at high levels of irregularity ($0.34 \sim 0.51$). This trend could indicate the existence of a threshold effect of irregularity where compressive strength would be improved when the irregularity exceeded a certain value. The strength enhancement phenomenon could be attributed to elimination of the natural fault planes that commonly occur in ordered structures .[10] The low level irregularity increased the instability of porous structure. When the irregularity exceeded a certain value, a new stress balance would be established. This could reduce the local stress concentration. The contradiction between stiffness and strength could be resolved by understanding the threshold of irregularity. This would result in porous structures with high strength and low stiffness being obtained.

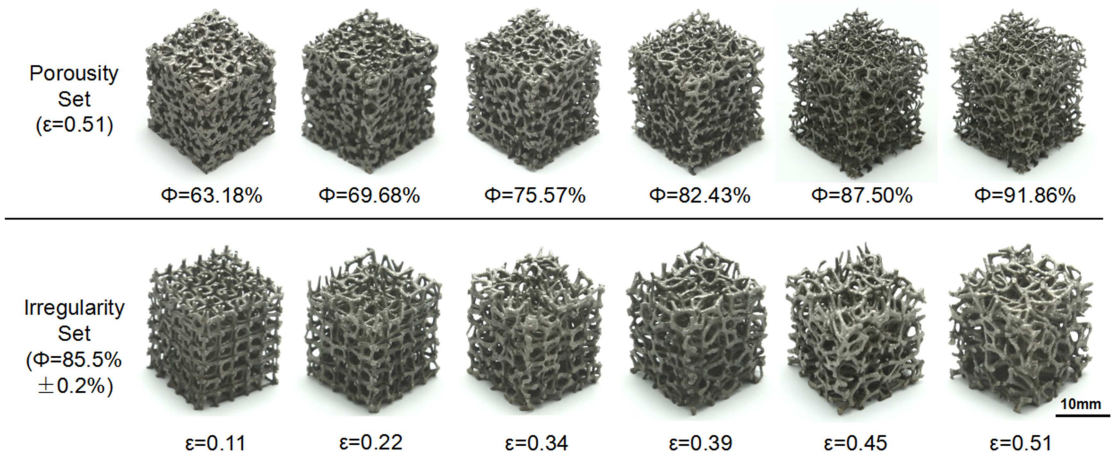

Figure 11: Porous specimens with different porosities and irregularities.

Table 3: Porosity of models and specimens of porous structure

Series		Porousity/%		Deviation/%
		Model	Specimen	
Porosity Series	1	64.77	63.18	2.45
	2	71.83	69.68	2.99
	3	78.46	75.57	3.69
	4	85.66	82.43	3.77
	5	90.24	87.50	3.03
	6	93.91	91.86	2.18
Irregularity Series	1	86.26	84.89	1.59
	2	85.75	83.92	2.14
	3	85.50	83.66	2.16
	4	85.44	84.05	1.63
	5	85.50	83.83	1.96
	6	85.69	83.67	2.36

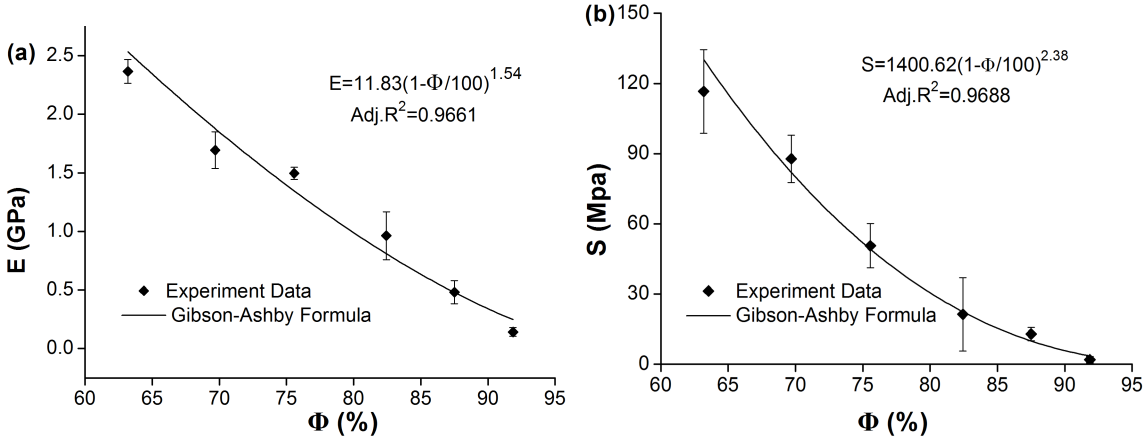

Figure 12: Relation between porosity and (a) elastic modulus, and (b) compressive strength.

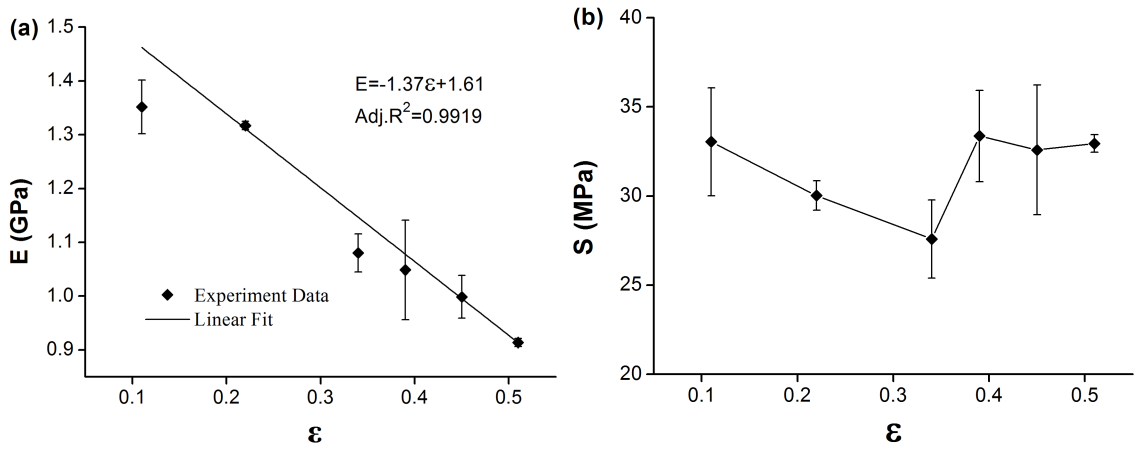

Figure 13: Relation between irregularity and (a) elastic modulus, and (b) compressive strength.

There has been plenty of past researches performed on the mechanical properties of irregular porous structures. The Gibson-Ashby model[21] model is a typical model that simplified the irregular porous structure into the regular structure built by the stacking of a special basic unit. Research discovered the following functions between porosity, elastic modulus, and compressive strength:

$$S = k\left(1 - \frac{\Phi}{100}\right)^m S_0, E = k\left(1 - \frac{\Phi}{100}\right)^m E_0 \tag{7}$$

Where, S_0 and E_0 is the compressive strength and elastic modulus of substrate materials, k is a constant related to mechanical properties of substrate materials.

When the irregularity of porous scaffolds is given, the mechanical properties are in accordance with the Gibson-Ashby model. However, when the irregularity is accounted for, the Gibson-Ashby model is no longer applicable. The Gibson-Ashby model is based on the regular assumption, ignoring the influence of irregularity in principle. It cannot reflect the change trend of the irregular effect on the mechanical properties. The results from the current study demonstrate that when the influence of irregularity is considered, the mechanical properties of porous structures should be at least three variable function parameters of the solid material (porosity, irregularity, and mechanical), that is $S = f(\Phi, \varepsilon, S_0), E = f(\Phi, \varepsilon, E_0)$.

The special mechanical behaviors of irregular porous scaffolds were also attributed to the SLM process. The process of the powered melting from the laser with high power density point by point occurred during the formation and solidification of the molten pools. The pores and cracks that occurred in specimens were inevitable. These cracks have a significant influence on their mechanical properties, especially on the compressive strength. [23,24] This resulted in a large data scatter within compressive testing. Moreover, previous studies [25,26] indicated that these defects were related to the orientation of the struts. As a result, subsequent research should focus on the orientation effect of the mechanical properties of sub-millimeter structures fabricated by SLM, as well as the threshold effect of the strength enhancement.

4. Conclusion

This study proposed a probability sphere method in order to construct irregular structures based on the Voronoi-Tessellation method. The porous specimens were fabricated by SLM. Their compressive behaviors were investigated. Our findings are summarized as follows:

(1) This method allowed us to obtain not only an accurate design of the specific porosity, as well as the gradient distribution of porosity. Porous scaffolds with special porosities ranging from 60% to 95 % and pore size ranging from 200 μm to 1200 μmwere designed precisely and conveniently. A porosity gradient ranging from 0.03 to 0.54 was obtained.

(2) The proposed irregular coefficient could control the irregularity of the porous structures and achieve good accommodation and balance of 'irregularity' and 'controllability'.

(3) The compressive properties were affected by both porosity and irregularity. The compressive strength decayed at low levels of irregularity. The compressive strength was enhanced at high levels, which enabled us to obtain porous structure with high strength but low stiffness.

(4) The compressive properties of porous structures could be adjusted to the level of cortical bone. The apparent elastic moduli of porous specimens had high irregularity (0.51) that varied from 0.14 Gpa to 2.37 Gpa. The compressive strengths varied from 1.94 Mpa to 116.61 Mpa.

Acknowledgement

The authors would like to thank the Key Research and Development Plan of Jiangsu Province (No., BE2016010-3), Science and Technology Support Program (The Industrial Part), Jiangsu Provincial Department of Science and Technology of China (No., BE2014009-1), the Science and Technology Supporting Plan (The Industrial Part) of Zhangjiagang (No., ZKG1615), the Science and Technology Supporting Plan (Social Development Part) of Zhangjiagang (No., ZKS1606), the Nation Nature Science Fund of China (No., 51475238).

References

(1) Geetha, M.; Singh, A. K.; Asokamani, R.; Gogia, A. K. *Progress in Materials Science* **2009**, *54*, 397–425.

(2) Niinomi, M.; Nakai, M. *International Journal of Biomaterials* **2011**, *2011*, 836587.

(3) Habibovic, P.; Yuan, H.; Cm, V. D. V.; Meijer, G.; van Blitterswijk, C. A.; De, G. K. *Biomaterials* **2005**, *26*, 3565–3575.

(4) Otsuki, B.; Takemoto, M.; Fujibayashi, S.; Neo, M.; Kokubo, T.; Nakamura, T. *Biomaterials* **2006**, *27*, 5892.

(5) Mastrogiacomo, M.; Scaglione, S.; Martinetti, R.; Dolcini, L.; Beltrame, F.; Cancedda, R.; Quarto, R. *Biomaterials* **2006**, *27*, 3230–3237.

(6) Wang, Z.; Wang, C.; Li, C.; Qin, Y.; Zhong, L.; Chen, B.; Li, Z.; Liu, H.; Chang, F.; Wang, J. *Journal of Alloys & Compounds* **2017**, *717*, 271–285.

(7) Liu, Y. J.; Li, X. P.; Zhang, L. C.; Sercombe, T. B. *Materials Science & Engineering A* **2015**, *642*, 268–278.

(8) Z, G. K.; M, S.; S, D.; JP, K.; H, W.; AA, Z.; S, A. Y. *Acs Applied Materials & Interfaces* **2016**, *9*, 1293.

(9) Wang, X.; Xu, S.; Zhou, S.; Xu, W.; Leary, M.; Choong, P.; Qian, M.; Brandt, M.; Xie, Y. M. *Biomaterials* **2016**, *83*, 127.

(10) Mullen, L.; Stamp, R. C.; Brooks, W. K.; Jones, E.; Sutcliffe, C. J. *Journal of Biomedical Materials Research Part B Applied Biomaterials* **2009**, *89*, 325–334.

(11) Yang, N.; Gao, L.; Zhou, K. *Materials Science & Engineering C Materials for Biological Applications* **2015**, *56*, 444–450.

(12) Gómez, S.; Vlad, M.; López, J.; Fernández, E. *Acta Biomaterialia* **2016**, *42*, 341–350.

(13) Sogutlu, S.; Koc, B. *Computer-Aided Design and Applications* **2007**, *4*, 661–670.

(14) Cai, S.; Xi, J. *Computer-Aided Design* **2008**, *40*, 1040–1050.

(15) Lal, P.; Sun, W. *Computer-Aided Design* **2004**, *36*, 487–497.

(16) Okabe, A.; Boots, B.; Sugihara, K.; Chiu, S. N. *Spatial Tessellations: Concepts and Applications of Voronoi Diagrams*; John Wiley & Sons, Inc., 2000; pp 357–363.

(17) Wejrzanowski, T.; Skibinski, J.; Szumbarski, J.; Kurzydlowski, K. J. *Computational Materials Science* **2013**, *67*, 216–221.

(18) Randrianalisoa, J.; Baillis, D.; Martin, C. L.; Dendievel, R. *International Journal of Thermal Sciences* **2015**, *98*, 277–286.

(19) Zhang, X.; Tang, L.; Liu, Z.; Jiang, Z.; Liu, Y.; Wu, Y. *Mechanics of Materials* **2016**, *104*, 73–84.

(20) Xiao, F.; Yin, X. *Computers & Mathematics with Applications* **2016**, *72*, 328–348.

(21) Gibson, L. J. A. A.; Ashby, M. F. *Cambridge University Press* **1998**, *33*, 487–488.

(22) Stamboulis, A. G.; Boccaccini, A. R.; Hench, L. L. *Advanced Engineering Materials* **2002**, *4*, 105–109.

(23) Popovich, A.; Sufiiarov, V.; Borisov, E.; Polozov, I. *Key Engineering Materials* **2015**, *651-653*, 677–682.

(24) Weißmann, V.; Bader, R.; Hansmann, H.; Laufer, N. *Materials & Design* **2016**, *95*, 188–197.

(25) Craeghs, T.; Clijsters, S.; Yasa, E.; Bechmann, F.; Berumen, S.; Kruth, J. P. *Optics & Lasers in Engineering* **2011**, *49*, 1440–1446.

(26) Wauthle, R.; Vrancken, B.; Beynaerts, B.; Jorissen, K.; Schrooten, J.; Kruth, J. P.; Humbeeck, J. V. *Additive Manufacturing* **2015**, *5*, 77–84.

Graphical TOC Entry